Journal of the Optical Society of America B

OPTICAL PHYSICS

Enhancing the sensitivity of an atom interferometer to the Heisenberg limit using increased quantum noise

RENPENG FANG,[1,*] RESHAM SARKAR,[1] AND SELIM M. SHAHRIAR[1,2]

[1]Department of Physics and Astronomy, Northwestern University, 2145 Sheridan Road, Evanston, Illinois 60208, USA
[2]Department of ECE, Northwestern University, 2145 Sheridan Road, Evanston, Illinois 60208, USA
*Corresponding author: renpengfang2016@u.northwestern.edu

Received 29 April 2020; accepted 6 May 2020; posted 14 May 2020 (Doc. ID 396358); published 11 June 2020

In a conventional atomic interferometer employing N atoms, the phase sensitivity is at the standard quantum limit: $1/\sqrt{N}$. Under usual spin squeezing, the sensitivity is increased by lowering the quantum noise. It is also possible to increase the sensitivity by leaving the quantum noise unchanged while producing phase amplification. Here we show how to increase the sensitivity, to the Heisenberg limit of $1/N$, while increasing the quantum noise by $\sqrt{N}$ and amplifying the phase by a factor of N. Because of the enhancement of the quantum noise and the large phase magnification, the effect of excess noise is highly suppressed. The protocol uses a Schrödinger cat state representing a maximally entangled superposition of two collective states of N atoms. The phase magnification occurs when we use either atomic state detection or collective state detection; however, the robustness against excess noise occurs only when atomic state detection is employed. We show that for one version of the protocol, the signal amplitude is N when N is even, and is vanishingly small when N is odd, for both types of detection. We also show how the protocol can be modified to reverse the nature of the signal for odd versus even values of N. Thus, for a situation where the probability of N being even or odd is equal, the net sensitivity is within a factor of $\sqrt{2}$ of the Heisenberg limit. Finally, we discuss potential experimental constraints for implementing this scheme via one-axis-twist squeezing employing the cavity feedback scheme, and show that the effects of cavity decay and spontaneous emission are highly suppressed because of the increased quantum noise and the large phase magnification inherent to the protocol. As a result, we find that the maximum improvement in sensitivity can be close to the ideal limit for as many as 10 million atoms.

https://doi.org/10.1364/JOSAB.396358

1. INTRODUCTION

In an atomic interferometer, the signal S can be expressed as a function of the phase difference ϕ between the two arms. The measurement sensitivity Λ can be expressed as the inverse of the phase fluctuation: $\Lambda = |\partial_\phi S/\Delta S|$, where $\partial_\phi \equiv \partial/\partial\phi$. Here, $\partial_\phi S$ is the phase gradient of the signal and ΔS is the noise, expressed as the standard deviation of the signal. When excess noise is suppressed sufficiently, Λ represents the inverse of the quantum phase fluctuation, limited by the quantum projection noise [1]. For a conventional atomic interferometer, the sensitivity is at the standard quantum limit (SQL): $\Lambda = \sqrt{N}$, with N being the number of atoms interrogated within the measurement time. Using spin squeezing, it is possible to surpass the SQL, and a key goal in this context is to achieve the Heisenberg limit (HL), under which $\Lambda = N$, representing an improvement by a factor of $\sqrt{N}$.

To enhance Λ, one can either increase the phase gradient or decrease the noise. In a conventional approach for spin squeezing, one minimizes the noise. For example, using optimal one-axis-twist squeezing and two-axis-counter-twist squeezing [2], the noise can be reduced respectively by a factor of $N^{1/3}$ and $\sqrt{N/2}$, while the phase gradient remains essentially unchanged. As such, $\Lambda = N^{5/6}$ for the former and $\Lambda = N/\sqrt{2}$ for the latter. Though the two-axis-counter-twist squeezing can yield a better sensitivity, it is experimentally more complicated than the one-axis-twist squeezing [3–10]. Recently, it was shown that it is also possible to reach sensitivity at or near the HL using variants of one-axis-twist squeezing [11–13]. Reference [11] proposed and Ref. [12] demonstrated the echo squeezing protocol, which can increase the phase gradient by a factor of $\sim\sqrt{N/e}$ while leaving the noise unchanged, thus producing $\Lambda \approx N/\sqrt{e}$. In Ref. [13] we proposed a Schrödinger cat atomic interferometer (SCAIN) that makes use of critically tuned one-axis-twist squeezing, rotation, inverse rotation and unsqueezing, and collective state detection [14–18]; it reduces the noise by a factor of $\sqrt{N}$ while leaving the phase gradient unchanged, yielding $\Lambda = N$.

In this paper, we describe a protocol that is a variant of the SCAIN protocol, with radically different behavior. It employs the conventional detection technique by measuring directly the populations of the spin-up or spin-down states of individual atoms. We show that under this protocol, the phase gradient is increased by a factor of N, while the noise is also increased by a factor of $\sqrt{N}$. The net enhancement of Λ is by a factor of $\sqrt{N}$, reaching the HL. However, because of the increase in noise, this is now significantly more robust to excess noise than all the protocols described above. Specifically, for this protocol, it should be possible to achieve $\Lambda = N/\sqrt{2}$ even when the excess noise is greater than the quantum projection noise for a conventional atom interferometer by a factor of $\sqrt{N}$. We also show that the signal amplitude is N when N is even, and is vanishingly small when N is odd, for both types of detection. In addition, we show how the protocol can be modified to reverse the nature of the signal for odd versus even values of N. Thus, for a situation where the probability of N being even or odd is equal, the net sensitivity is within a factor of $\sqrt{2}$ of the HL. Finally, we discuss potential experimental constraints for implementing this scheme via one-axis-twist squeezing employing the cavity feedback scheme, and show that the effects of cavity decay and spontaneous emission are highly suppressed due to the increased quantum noise and the large phase magnification inherent to the protocol.

The rest of the paper is organized as follows. In Section 2 we describe the protocol for the increased-noise SCAIN employing conventional detection. In Section 3, we present the analytical derivations of signals, noise, and enhancement of sensitivity under conventional detection and collective state detection. In Section 4, we discuss the suppression of the effect of excess noise. In Section 5 we discuss experimental considerations, and estimate the effect of cavity decay and spontaneous emission, with some of the details of the analysis presented in Appendix A. In Section 6, we discuss comparisons with other protocols [19–21] that are closely related to ours. We present the conclusion in Section 7.

2. SCHRÖDINGER CAT ATOMIC INTERFEROMETER WITH INCREASED NOISE

The protocol considered here is a modified version of the SCAIN, which is based on the conventional Raman atomic interferometer [22–25]. Briefly, both make use of N three-level atoms with metastable states $|1, p_z = 0\rangle$ and $|2, p_z = \hbar k\rangle$ and an excited state $|3\rangle$ in the Λ configuration, coupled by a pair of counterpropagating laser beams. Here, $k \equiv k_1 + k_2$, with k_1 (k_2) being the wavenumber for the beam propagating in the $+\hat{z}$ ($-\hat{z}$) direction, and p_z is the z component of the linear momentum of the atom. Each atom can be reduced to an equivalent two-level model via adiabatic elimination of the excited state [26,27], and thus can be represented by a pseudospin-1/2 operator $\hat{\boldsymbol{j}}$, where we define $|\downarrow\rangle \equiv |1, p_z = 0\rangle$ and $|\uparrow\rangle \equiv |2, p_z = \hbar k\rangle$. The ensemble, represented by a collective spin operator $\hat{\boldsymbol{J}} \equiv \sum_i^N \hat{\boldsymbol{j}}_i$, is initially prepared in a coherent spin state [15], $|-\hat{\boldsymbol{z}}\rangle = \prod_{i=1}^N |\downarrow\rangle$, where all atoms

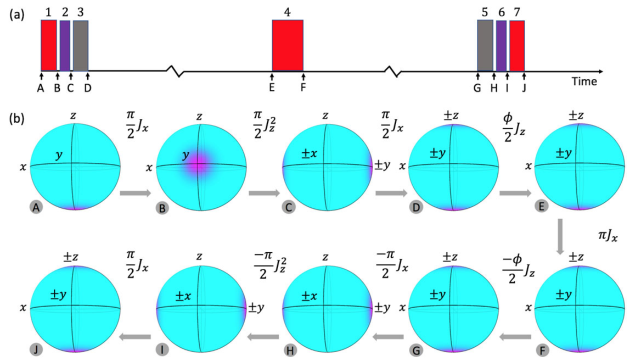

Fig. 1. (a) Schematic illustration of the protocol employed for the Schrödinger cat atomic interferometer, (b) the Husimi quasi-probability distributions at different stages of the protocol, for $N = 40$, $\mu = \pi/2$, auxiliary rotation axis $= \hat{\boldsymbol{x}}$, $\xi = -1$, and $\phi = 0.5\pi/N$.

are in the spin-down state. Here we employ the notation that a state $|\hat{\boldsymbol{e}}\rangle$ is a coherent spin state in the direction of the unit vector $\hat{\boldsymbol{e}}$, with the pseudospin vector of each atom being in that direction. For the conventional Raman atomic interferometer, the ensemble is then subjected to the usual pulse sequence of $\pi/2$—dark—π—dark—$\pi/2$, labeled 1, 4, 7 in Fig. 1(a). For the SCAIN, however, the ensemble undergoes four additional pulses, labeled 2, 3, 5, 6 in Fig. 1(a), corresponding to the squeezing, rotation, inverse rotation, and unsqueezing operations [13].

The evolution of the quantum states on a Bloch sphere is shown in Fig. 1(b), using the Husimi quasi-probability distribution [2,15]. The exact effects of the protocol depend on the values of a set of parameters: the parity of N, the squeezing parameter μ for one-axis-twist squeezing, the auxiliary rotation axis (which can be $\hat{\boldsymbol{x}}$ or $\hat{\boldsymbol{y}}$) around which the rotation will be implemented, the corrective rotation sign ξ, which can take values of ± 1 corresponding to redoing or undoing the first auxiliary rotation, and the dark zone phase shift ϕ. The case shown here is for an even value of $N = 40$, with $\mu = \pi/2$, auxiliary rotation axis $= \hat{\boldsymbol{x}}$, $\xi = -1$, and $\phi = \pi/80$. In our notation, the quasi-probability distribution for a state $|\Psi\rangle$ is expressed as $Q_H(\theta, \phi) \equiv |\langle\Psi|\Phi(\theta, \phi)\rangle|^2$, where

$$|\Phi(\theta, \phi)\rangle \equiv \left(\cos\frac{\theta}{2}\right)^N \sum_{k=0}^{N} \sqrt{\binom{N}{k}} \left(e^{i\phi} \tan\frac{\theta}{2}\right)^k |E_{N-k}\rangle \tag{1}$$

represents the coherent spin state corresponding to all the spins pointing in the direction $\{\theta, \phi\}$, and $|E_n\rangle$ represents the Dicke collective states [14–16], defined as

$$|E_n\rangle = \sum_{k=1}^{\binom{N}{n}} P_k |\downarrow^{N-n} \otimes \uparrow^n\rangle \Big/ \sqrt{\binom{N}{n}}, \tag{2}$$

with P_k being the permutation operator [16,28]. Here, the extremal state $|E_N\rangle$ corresponds to all pseudospins in the $\hat{\boldsymbol{z}}$ direction. As such, we will refer to these as the Z-directed Dicke manifold. As needed, we will also refer to $X(Y)$-directed Dicke manifolds, for which $|E_N\rangle$ corresponds to all pseudospins in the $\hat{\boldsymbol{x}}$ ($\hat{\boldsymbol{y}}$) direction.

In illustrating the nature of the quasi-probability distribution at various stages, we have used different orientations of the Bloch sphere as appropriate, and added $\pm$ symbols in front of two axes to indicate that the picture looks the same when it is rotated by 180° around the third axis. At the start (point A), the system is in state $|-\hat{\boldsymbol{z}}\rangle$. After the first $\pi/2$ pulse (point B), the state rotates around the $\hat{\boldsymbol{x}}$ axis to reach state $|\hat{\boldsymbol{y}}\rangle$. We then apply a squeezing Hamiltonian of the form $H = \chi \hat{J}_z^2$ for a duration of τ such that $\mu = \chi\tau$. After the squeezing pulse (point C), the state is split equally between two coherent spin states, and can be expressed as $(|\hat{\boldsymbol{y}}\rangle - \eta|-\hat{\boldsymbol{y}}\rangle)/\sqrt{2}$ [29–33], where $\eta = i(-1)^{N/2}$, representing a phase factor with unity amplitude. It should be noted that this phase factor depends on the super-even parity, representing whether $N/2$ is even or odd; however, the shapes of the fringes, as well as the values of the quantum phase fluctuation, are not expected to depend on the value of the super-even parity, as we have verified explicitly.

This is a cat state [34], but as a superposition of the two extremal states of the Y-directed Dicke manifold, which cannot be used to achieve phase magnification, since the phase difference between the two arms corresponds to rotation around the $\hat{\boldsymbol{z}}$ axis. This problem is solved by applying the auxiliary rotation of $\pi/2$ around the $\hat{\boldsymbol{x}}$ axis, which transforms this state to $(|-\hat{\boldsymbol{z}}\rangle + \eta|\hat{\boldsymbol{z}}\rangle)/\sqrt{2}$. This (point D) represents the desired cat state, as a superposition of the two extremal states of the Z-directed Dicke manifold: $(|E_0\rangle + \eta|E_N\rangle)/\sqrt{2}$. After the first dark zone (point E), the state is $e^{-i\phi\hat{J}_z/2}(|E_0\rangle_L + \eta|E_N\rangle_U)/\sqrt{2}$, where the subscript L (U) is for the lower (upper) arm of the interferometer. Since both $|E_0\rangle$ and $|E_N\rangle$ are eigenstates of $\hat{J}_z$, with eigenvalues of $-N/2$ and $N/2$, respectively ($\hbar = 1$), this state can be simplified to $(e^{i\phi N/4}|E_0\rangle_L + e^{-i\phi N/4}\eta|E_N\rangle_U)/\sqrt{2}$. The resulting quasi-probability distribution remains unchanged, but the quantum state incorporates these phase accumulations. After the π pulse (point F), $|E_0\rangle_L$ becomes $-i|E_N\rangle_L$, while $|E_N\rangle_U$ becomes $-i|E_0\rangle_U$. After the second dark zone (point G), the state is $(e^{i\phi N/2}\eta|E_N\rangle_L + e^{-i\phi N/2}|E_0\rangle_U)/\sqrt{2}$, so that the net phase difference between the two paths is $N\phi$, thus magnifying the rotation-induced phase by a factor of N. To reveal the phase magnification, we apply another auxiliary rotation by an angle of $-\pi/2$ around the $\hat{\boldsymbol{x}}$ axis (point H), followed by the unsqueezing Hamiltonian, $-H$ (point I). After the second $\pi/2$ pulse (point J), the state is $|\Psi\rangle_f = \cos(N\phi/2)|E_0\rangle - \eta\sin(N\phi/2)|E_N\rangle$. The whole protocol can be expressed as

$$|\Psi\rangle_f = e^{-i\frac{\pi}{2}\hat{J}_x} e^{i\mu\hat{J}_z^2} e^{-i\xi\frac{\pi}{2}\hat{J}_x} e^{i\frac{\phi}{2}\hat{J}_z} e^{-i\pi\hat{J}_x} \times e^{-i\frac{\phi}{2}\hat{J}_z} e^{-i\frac{\pi}{2}\hat{J}_x} e^{-i\mu\hat{J}_z^2} e^{-i\frac{\pi}{2}\hat{J}_x}|-\hat{\boldsymbol{z}}\rangle. \quad (3)$$

If the population of the collective state $|E_0\rangle$ were detected [13], the signal would be $\cos^2(N\phi/2)$, with fringes a factor of N narrower than that for the conventional Raman atomic interferometer. The phase gradient remains unchanged, since the phase enhancement is countered by a reduction in the signal amplitude by a factor of N. However, the noise is now reduced by a factor of $\sqrt{N}$, since the number of particles is unity. As such, the sensitivity increases by $\sqrt{N}$, reaching the HL. In what follows, we show how the behavior of the interferometer is altered very significantly when we employ the conventional detection technique corresponding to measuring the z component of the combined spin of all atoms, the $\hat{J}_z$ operator, which represents the difference between the number of atoms in the spin-up and spin-down states.

The signal for the conventional detection SCAIN is obtained by expanding $\hat{J}_z$ in the basis of the Z-directed Dicke manifold, and then taking the expectation value with respect to $|\Psi\rangle_f$. This is found to be $\langle\Psi_f|\hat{J}_z|\Psi_f\rangle = -N/2\cos(N\phi)$, as derived in Section 3, again showing N-fold fringe narrowing. However, compared to the case of the collective state detection SCAIN, the amplitude of the fringes is now a factor of N larger. As such, the phase gradient is now larger than that for a conventional Raman atomic interferometer by a factor of N. At the same time, the noise is also increased by a factor of $\sqrt{N}$, as derived in Section 3. The net enhancement in sensitivity is by a factor of $\sqrt{N}$, reaching the HL, just as in the case of the collective state detection SCAIN. However, because of the increase in quantum noise, the conventional detection SCAIN is significantly more robust against excess noise, as discussed in Section 4.

For the particular choice of the auxiliary rotation axis used in the protocol in Fig. 1(b), the expression for the signal for the conventional detection SCAIN shown above applies only to the case when N is even. The results for the odd value of $N = 41$, with all other parameters the same as in Fig. 1(b), are found to be drastically different (see Section 3), due to the fact that the state after the squeezing pulse will now be split equally between $|\hat{\boldsymbol{x}}\rangle$ and $|-\hat{\boldsymbol{x}}\rangle$, thus generating a cat state as a superposition of the two extremal states of the X-directed Dicke manifold [29–31]. This modification of the state, caused by a change of just 1 in the value of N, can be understood by noting that the propagator corresponding to the one-axis-twist squeezing Hamiltonian for $\mu = \pi/2$ can be decomposed as a sum of two parts, one of which is proportional to a product of N Pauli spinors [30,31]. The ensuing auxiliary rotation around the x axis will not transform it into the desired cat state required to yield the N-fold phase amplification. This also complicates the evolution of the quantum states during the following stages, for which an analytical expression for the final state is not easy to find. Instead, we take a numerical approach to simulating the state evolutions [35]. The signals for the conventional detection SCAIN as a function of ϕ, for both even and odd values of N, are shown in Fig. 2; for reference, the signal corresponding to one full fringe of the conventional Raman atomic interferometer is also shown in Fig. 2(a). The plots in Figs. 2(b) and 2(c) clearly show the N-fold narrowed fringes for the even case, while only a central fringe is observable for the odd case. We also find that changing the sign of ξ simply inverts the fringes, which implies that the N-fold reduction of the fringe width happens for the even case no matter whether we choose to redo ($\xi = 1$) or undo ($\xi = -1$) the first auxiliary rotation. Of course, the nature of the signals for odd and even values of N can be reversed by switching the choice of the auxiliary rotation axis from $\hat{\boldsymbol{x}}$ to $\hat{\boldsymbol{y}}$.

In Fig. 3, we illustrate the behavior of the inverse of the quantum fluctuation in rotation (QFR^{-1}) as a function of the squeezing parameter μ for different choices of parameters for

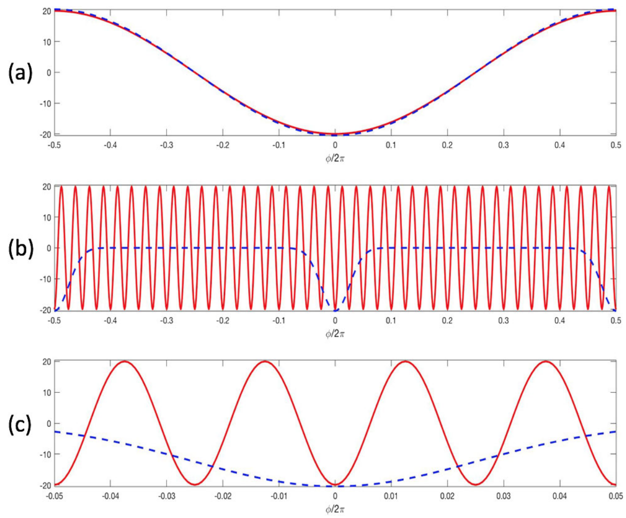

Fig. 2. Signals corresponding to the detection of $\langle \hat{J}_z/\hbar \rangle$ as a function of ϕ, for $\mu = \pi/2$, auxiliary rotation axis $= \hat{\boldsymbol{x}}$, and $\xi = -1$. $N = 40$ is shown in red, while $N = 41$ is shown by the dashed blue curves. (a) Fringes for conventional Raman atomic interferometer for comparison, (b) fringes for the conventional detection SCAIN, (c) zoomed-in view of the fringes shown in (b). The horizontal span in (c) is 10 times smaller than those in (a) and (b).

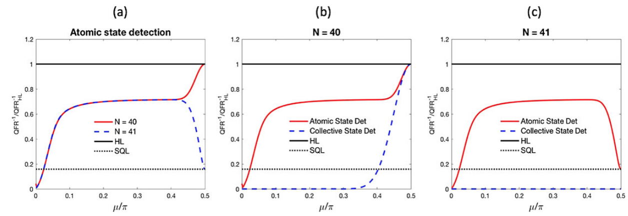

Fig. 3. Illustration of QFR^{-1} for different cases as a function of the squeezing parameter μ, normalized to the HL (solid black line), for auxiliary rotation axis $= \hat{\boldsymbol{x}}$ and $\xi = +1$. (a) The case of the conventional detection SCAIN, with red for $N = 40$ and the dashed blue curve for $N = 41$, (b) comparison between the conventional detection SCAIN and the collective state detection SCAIN for an even $N = 40$, (c) similar comparison for an odd $N = 41$. The dotted black line shows the SQL.

the conventional detection SCAIN, along with a comparison with the collective state detection SCAIN. The quantum fluctuation in rotation is simply a scaled version of the quantum phase fluctuation when the phase difference is induced by rotation. For each case, QFR^{-1} is normalized to $\mathrm{QFR}_{\mathrm{HL}}^{-1}$ for $N = 40$, as indicated by the solid black line. The dashed black line shows the $\mathrm{QFR}_{\mathrm{SQL}}^{-1}$ values for $N = 40$. Figure 3(a) shows QFR^{-1} values for the conventional detection SCAIN only. For $\mu = \pi/2$, the sensitivity for an even number of atoms (red) is at the HL, and that for an odd number of atoms (dashed blue) is at the SQL. For an even N, this sensitivity is reached due to an amplification of the phase by a factor of N, and a concomitant increase in the noise by a factor of $\sqrt{N}$. For an odd N, there is a phase amplification, manifested as a Fabry–Perot-like fringe around $\phi = 0$ that is narrowed by a factor of $\sqrt{N}$, along with an increase in the noise by a factor of $\sqrt{N}$. The difference between the two cases disappears when the value of μ is reduced below a threshold value of $\sim 0.45\pi$. There is a range of values of the squeezing parameter $(0.2\pi \le \mu \le 0.45\pi)$ over which the normalized value of QFR^{-1} is $\sim 1/\sqrt{2}$. Finally, we note that the vanishing value of QFR^{-1} for $\mu = 0$ is simply due the fact that the signal is constant as a function of ϕ. In Figs. 3(b) and 3(c), we compare the sensitivity of the conventional detection SCAIN with that of the collective state detection SCAIN for even and odd N values, respectively. For an even N value, the sensitivity for both detection protocols are the same for $\mu = \pi/2$. However, for the collective state detection SCAIN, the sensitivity drops off to zero rapidly for decreasing values of μ. For an odd value of N, the sensitivity for the collective state detection SCAIN is zero for all values of μ, due to the signal being a constant as a function of ϕ.

Until now, we have analyzed and compared the performance of a conventional detection SCAIN separately for even and odd values of N. In scenarios where the odd and even parity cases can occur with equal probability (for example, when atoms caught in a magneto-optic trap and then released are used as the source for the conventional detection SCAIN), the average value of QFR^{-1} is given by $\mathrm{QFR}_{\mathrm{AVE}}^{-1} = [(\mathrm{QFR}_{\mathrm{EVEN}}^{-1})^2/2 + (\mathrm{QFR}_{\mathrm{ODD}}^{-1})^2/2]^{1/2}$ [35]. Thus, for a large number of atoms ($N \gg 1$), the average sensitivity is a factor of $\sqrt{2}$ below the HL.

As described in Ref. [18], the combination of one-axis-twist squeezing, rotation, unrotation, unsqueezing, and collective state detection can also be used to realize a Schrödinger cat (SC) atomic clock with HL sensitivity. Such a clock with HL sensitivity can also be realized when conventional detection of atomic states is employed, but with increased quantum noise, thus making it highly insensitive to excess noise [35].

3. ANALYTICAL DERIVATIONS OF SIGNALS, NOISE, AND ENHANCEMENT OF SENSITIVITY UNDER CONVENTIONAL DETECTION AND COLLECTIVE STATE DETECTION

As shown earlier, with the chosen parameters, the final state of the ensemble for the SCAIN protocol is given by $|\Psi\rangle_f = \cos(N\phi/2)|E_0\rangle - \eta \sin(N\phi/2)|E_N\rangle$. For collective state detection, the operator to be measured can be defined in general as $\hat{Q}_m \equiv |E_m\rangle\langle E_m|$, where $|E_m\rangle$ is the Dicke collective state defined in Eq. (2). Thus, the operator we measure is $\hat{Q}_0$ if we detect the $|E_0\rangle$ state, and $\hat{Q}_N$ if we detect the $|E_N\rangle$ state. For the final state described above, if we measure the former, the signal is $\cos^2(N\phi/2)$; if we measure the latter, the signal is $\sin^2(N\phi/2)$. For conventional detection, the operator we measure is $\hat{R} = \hat{J}_z/\hbar$. It can be shown [35] that $\hat{R} = \hat{J}_z/\hbar = \sum_{m=-J}^{J} m \hat{Q}_{J+m}$. In the final state described above, we have only two of the collective states. As such, for this state, $\langle \hat{R} \rangle = -J\langle \hat{Q}_0 \rangle + J\langle \hat{Q}_N \rangle$. Thus it follows that for conventional detection, the signal is given by $-J\cos^2(N\phi/2) + J\sin^2(N\phi/2) = -(N/2)\cos(N\phi)$, which has the same fringe width as that obtained by using collective state detection, except that the signal now ranges from $N/2$ to $-N/2$.

To determine QFR^{-1} for both protocols, we first define the signal for collective state detection as $\Sigma \equiv \langle \hat{Q}_0 \rangle =$

$\cos^2(N\phi/2)$ and the standard derivation of the signal as $\Delta\Sigma \equiv [\langle \hat{Q}_0^2\rangle - \Sigma^2]^{1/2}$. Similarly, we define the signal for conventional detection as $S \equiv \langle \hat{R}\rangle = -(N/2)\cos(N\phi)$ and the standard deviation of the signal as $\Delta S \equiv [\langle \hat{R}^2\rangle - S^2]^{1/2}$. Noting that $\phi = 2\,\mathrm{m}A\Omega_G/\hbar \equiv \Omega_G/\Gamma$, with A being the area of the whole interferometer and Ω_G being the normal component of the rate of rotation, we can now write

$$\mathrm{QFR}_Q^{-1} = \left|\Gamma^{-1}\frac{\partial\Sigma/\partial\phi}{\Delta\Sigma}\right|; \quad \mathrm{QFR}_R^{-1} = \left|\Gamma^{-1}\frac{\partial S/\partial\phi}{\Delta S}\right|, \quad \textbf{(4)}$$

where we have used the subscript Q for collective state detection and R for conventional detection. We note that $\hat{Q}_0^2 = \hat{Q}_0$, which means that $\Delta\Sigma \equiv [\Sigma - \Sigma^2]^{1/2}$. Using the expression for Σ from above, we easily find that $\mathrm{QFR}_Q^{-1} = N/\Gamma$. The value of QFR^{-1} for a conventional Raman atomic interferometer is given by $\sqrt{N}/\Gamma$, which is the SQL. As such, collective state detection represents an improvement by a factor of $\sqrt{N}$, reaching the HL sensitivity.

For conventional detection, it easy to show [35] that $\hat{R}^2 = \sum_{m=-J}^{J} m^2\,\hat{Q}_{J+m}$. Thus, for the final state described above, we get $\langle \hat{R}^2\rangle = J^2\langle \hat{Q}_0\rangle + J^2\langle \hat{Q}_N\rangle = J^2 = N^2/4$. It follows immediately that $\Delta S \equiv [\langle \hat{R}^2\rangle - S^2]^{1/2} = \{N^2/4 - N^2/4[\cos^2(N\phi)]\}^{1/2} = (N/2)|\sin(N\phi)|$. It should be noted that the peak value of the standard deviation of the signal in this case is $N/2$, which happens at the points where the slope of the fringe is the maximum. From Eq. (4), we then get $\mathrm{QFR}_R^{-1} = N/\Gamma$, yielding the HL sensitivity.

4. INSENSITIVITY TO EXCESS NOISE

The degree of suppression of excess noise for different protocols is illustrated in Fig. 4. Here, we consider a situation where excess noise contributes an additional variance ΔS_{EN}^2 to the signal. The sensitivity is then given by $\Lambda = |\partial_\phi S/\sqrt{\Delta S_{\mathrm{QPN}}^2 + \Delta S_{\mathrm{EN}}^2}| = \Lambda_{\mathrm{QPN}}/\sqrt{1+\rho^2}$, where $\rho \equiv \Delta S_{\mathrm{EN}}/\Delta S_{\mathrm{QPN}}$. Here we have use the subscript "EN" for excess noise and "QPN" for quantum projection noise.

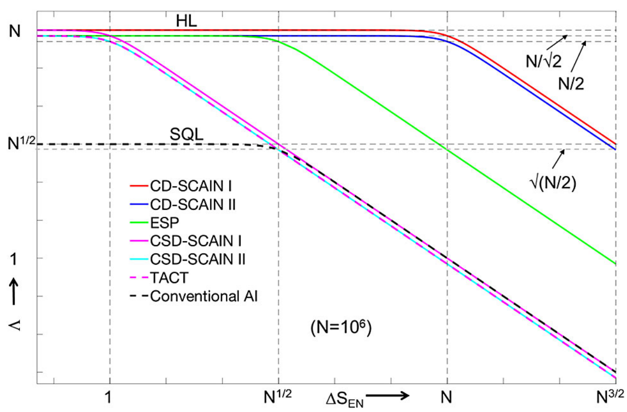

Fig. 4. Sensitivity Λ as a function of excess noise ΔS_{EN} for various protocols. CD, conventional detection; CSD, collective state detection; ESP, echo squeezing protocol; TACT, two-axis-counter-twist squeezing; AI, atomic interferometer. For each version of the SCAIN, I indicates the case when the parity of N is known, while II indicates the case where the signal is averaged over both parities.

One way to characterize the degree of robustness against excess noise is by determining the value of ΔS_{EN} for which $\rho = 1$. As can be seen, for two-axis-counter-twist squeezing, this value is 1, making it particularly vulnerable to excess noise. In contrast, for the echo squeezing protocol (as well as for the conventional atomic interferometer), this value is $\sqrt{N}$, making it a factor of $\sqrt{N}$ more robust than two-axis-counter-twist squeezing. For the conventional detection SCAIN, this value is N, making it a factor of $\sqrt{N}$ more robust that the echo squeezing protocol and a factor of N more robust than two-axis-counter-twist squeezing. We also see that the collective state detection SCAIN is as sensitive to excess noise as two-axis-counter-twist squeezing. Thus, in switching from collective state detection to conventional detection, the robustness of the SCAIN protocol to excess noise is improved by a factor of N. In Section 6, we discuss other protocols that have been proposed recently with insensitivities to excess noise comparable to that of the conventional detection SCAIN.

5. LIMITATIONS ON MAXIMUM ACHIEVABLE SENSITIVITY DUE TO EXPERIMENTAL NON-IDEALITIES

While ideally the conventional detection SCAIN would enhance the sensitivity by a factor of $\sqrt{N}$ and be robust against excess noise, various experimental non-idealities would potentially limit the maximal achievable sensitivity. We consider first the effect of non-idealities inherent in the one-axis-twist squeezing process needed for generating the SC state. There are several experimental schemes for realizing one-axis-twist squeezing [3,4,7,11,12,36–40]. For concreteness, here we consider the approach based on cavity feedback dynamics [3,4,7,11,12,37] and investigate the effects of cavity decay and spontaneous emission. In this approach, a probe is passed through a cavity at a frequency that is tuned halfway between the two legs of a Λ transition in which the spin-up and spin-down states are coupled to an intermediate state. The cavity is tuned to be below resonance for the probe. The energy levels of the spin-up and spin-down states are light shifted due to the probe, in opposite directions. The resulting dispersion shifts the cavity resonance frequency by an amount that is proportional to J_z. The intracavity probe intensity changes linearly with this cavity shift, since it is on the side of the resonance, thus affecting the light shifts. The net result is an energy shift for all the atoms that is proportional to J_z^2, so that the interaction Hamiltonian can be expressed as $H = \hbar\chi J_z^2$, where χ is a parameter that determines the strength of the squeezing process. Changing the sign of the probe detuning with respect to the cavity resonance reverses the sign of the Hamiltonian, thus producing unsqueezing. For a squeezing interaction time of τ, the characteristic strength for the process is given by $\mu \equiv \chi\tau$. This is illustrated schematically in Fig. 5. Here the detuning for the cavity mode with respect to either ground state is Δ, and the probe detuning with respect to the cavity resonance is δ.

In order to express the results quantitatively, we note first that while the actual improvement in the performance of the interferometer or the clock is given by $(\Lambda/\Lambda_{\mathrm{SQL}})$, it is customary in the literature to quote the value of $(\Lambda/\Lambda_{\mathrm{SQL}})^2$. To

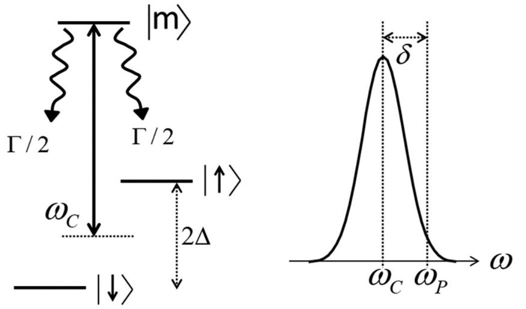

Fig. 5. Illustration of the scheme considered for one-axis-twist squeezing using a three-level system, where the two low-lying states are metastable and represent the spin-up and spin-down states.

remain consistent with this custom, we define $\mathcal{F}$, the factor of improvement, as follows:

$$\mathcal{F} \equiv \left(\frac{\Lambda}{\Lambda_{\mathrm{SQL}}}\right)^2 = \frac{(\Delta\phi_{\mathrm{SQL}})^2}{(\Delta\phi)^2} = \frac{(1/N)}{(\Delta\phi)^2}. \quad (5)$$

To incorporate the effects of cavity decay and spontaneous emission, we can write

$$(\Delta\phi)^2 = (\Delta\phi_{\mathrm{COH}})^2 + (\Delta\phi_{\mathrm{CAV}})^2 + (\Delta\phi_{\mathrm{SE}})^2, \quad (6)$$

where $\Delta\phi_{\mathrm{COH}}$ represents the phase variance due to the coherent evolution of the spins, $\Delta\phi_{\mathrm{CAV}}$ represents the phase variance due to cavity decay, and $\Delta\phi_{\mathrm{SE}}$ represents the phase variance due to spontaneous emission. Thus, we get

$$\mathcal{F} = [N\{(\Delta\phi_{\mathrm{COH}})^2 + (\Delta\phi_{\mathrm{CAV}})^2 + (\Delta\phi_{\mathrm{SE}})^2\}]^{-1}. \quad (7)$$

We also define $\Delta\phi_{\mathrm{IDL}}$ as the phase variance under ideal conditions (i.e., when there is no cavity decay or spontaneous emission). We recall that under these conditions, the signal for the conventional detection SCAIN is $S_{\mathrm{IDL}} = \langle \hat{J}_z \rangle = (-N/2)\mathrm{Cos}(N\phi)$, with $\Delta S_{\mathrm{IDL}} = (N/2)|\mathrm{Sin}(N\phi)|$ and $(\partial_\phi S)_{\mathrm{IDL}} = (N^2/2)\mathrm{Sin}(N\phi)$. Thus, in this case,

$$\Delta\phi_{\mathrm{COH}} = \Delta\phi_{\mathrm{IDL}} = \frac{\Delta S_{\mathrm{IDL}}}{|\partial_\phi S|_{\mathrm{IDL}}} = \frac{1}{N}, \quad (8)$$

independent of the value of ϕ, so that $\mathcal{F}_{\mathrm{IDL}} = N$. Of course, in general, $\Delta\phi_{\mathrm{COH}} \neq \Delta\phi_{\mathrm{IDL}}$.

For the general case where some of the spins are dephased due to either cavity decay or spontaneous emission, the number of atoms, defined as $\tilde{N}$, that will constitute the cat state, representing the coherent evolution of the spins, will be less than N. Thus, we can write the coherent part of the signal, its standard deviation, and its phase gradient as

$$\tilde{S} = (-\tilde{N}/2)\mathrm{Cos}(\tilde{N}\phi);\ \Delta\tilde{S} = (\tilde{N}/2)|\mathrm{Sin}(\tilde{N}\phi)|;$$
$$|\partial_\phi \tilde{S}| = (\tilde{N}^2/2)|\mathrm{Sin}(\tilde{N}\phi)|. \quad (9)$$

The angular variances are determined by the ratios of the signal variances and the phase gradients of the coherent part of the signal, as follows:

$$(\Delta\phi_{\mathrm{COH}})^2 = (\Delta\tilde{S})^2/(\partial_\phi\tilde{S})^2,$$
$$(\Delta\phi_{\mathrm{CAV}})^2 = (\Delta S_{\mathrm{CAV}})^2/(\partial_\phi\tilde{S})^2,$$
$$(\Delta\phi_{\mathrm{SE}})^2 = (\Delta S_{\mathrm{SE}})^2/(\partial_\phi\tilde{S})^2. \quad (10)$$

As illustrated in Fig. 2 of Ref. [1], during the operation of an interferometer, one measures the signal at two different phases, $(\phi - \delta\phi)$ and $(\phi + \delta\phi)$, and ϕ is varied until these two signals are equal. The value of ϕ determined this way corresponds to the value for which the signal is the maximum. Deviation of this value of ϕ from the quiescent value (typically zero) is then used to determine the amount of rotation in the case of an atom interferometric gyroscope. For the conventional detection SCAIN, a convenient value of $\delta\phi$ is $\pi/(2\tilde{N})$. This corresponds to making measurements at the point of the signal fringe where both the magnitude of the phase gradient of the coherent signal ($|\partial_\phi\tilde{S}|$) and the standard deviation of the coherent signal ($\Delta\tilde{S}$) have their maximum values, as can be seen in Eq. (9). Therefore, all quantities in Eq. (10) are to be evaluated at $\phi_o = \pi/(2\tilde{N})$. We thus get

$$\mathcal{F} = \left[\frac{4N}{\tilde{N}^4}\left\{\frac{\tilde{N}^2}{4} + (\Delta S_{\mathrm{CAV}})^2 + (\Delta S_{\mathrm{SE}})^2\right\}\right]^{-1}. \quad (11)$$

It should be noted that the effect of the variances due to cavity decay as well as due to spontaneous emission are strongly suppressed because of the magnified phase gradient of the signal. This is yet another manifestation of the robustness of the conventional detection SCAIN.

We use $\delta N \equiv N - \tilde{N}$ to represent the reduction in the peak-to-peak amplitude of the signal due to non-idealities. As we show next, the cavity decay process and the spontaneous emission process both contribute to δN, along with producing additional variances in the signal. The net reduction in the value of $\mathcal{F}$ is due to a combination of these factors. In what follows, we estimate the values of ΔS_{CAV}, ΔS_{SE}, and δN resulting from these processes, in order to determine the value of $\mathcal{F}$. Note that the following analysis makes frequent use of parameters defined and equations derived in Appendix A.

Consider first the effect of cavity decay. A rigorous study of the effect of cavity decay on the SCAIN protocol would require carrying out the whole analysis using the density matrix approach, based on the Hamiltonian and the Lindblad operator shown in Eq. (A10) in Appendix A. For N atoms, the size of the density matrix will be N^2. To solve the equation of motion, one has to form a vector consisting of all the elements of the density matrix, and the propagator matrix that determines the time derivative of this vector would have dimensions of $N^2 X N^2$ [41]. This is a daunting task for a large value of N. For example, to determine the time evolution for $N = 10^3$, one has to diagonalize a matrix with 10^{12} elements. Diagonalization is necessary even if one wants to make use of direct numerical integration, since the smallest time steps to be used for the integration must be significantly smaller than the inverse of the largest eigenvalue of the propagator matrix, and the duration of the evolution must be significantly larger than the inverse of the smallest eigenvalue. In the near future, we will carry out such an analysis for as large a value of N as feasible within the constraints of computation resources. For the present work, we make use of a perturbative approach consisting of two steps. In the first step, we ignore the effect of the cavity decay and use the Hamiltonian of Eq. (A10) to evolve the quantum state of the ensemble coherently. The results of this step have already been documented above. In the second step, we estimate the effect of the cavity decay by considering the density matrix equation of motion attributable to only the Lindblad operator in Eq. (A10). Such a two-step approach has also been used in Ref. [11], for example. Below we carry out the second step of this analysis.

We define $\gamma \equiv 2\chi/\tilde{\delta}$ (where $\tilde{\delta}$ is the probe detuning normalized to the cavity decay rate) so that the Lindblad operator in Eq. (A10) can be expressed as $L = \sqrt{\gamma} J_z$. From Eq. (A5), it then follows that the incoherent part of the evolution of the density matrix can be written as

$$\dot{\rho} = \gamma J_z \rho J_z^\dagger - \frac{\gamma}{2}\{J_z^\dagger J_z, \rho\}. \tag{12}$$

Using the fact that $\langle \dot{\hat{O}} \rangle = tr(\dot{\rho}\hat{O})$ for any operator $\hat{O}$, it can be shown that

$$\begin{aligned} &\langle \dot{J}_\pm \rangle = -(\gamma/2)\langle J_\pm \rangle, \\ &\langle \dot{J}_x^2 \rangle = -\gamma \langle J_x^2 \rangle + \gamma \langle J_y^2 \rangle; \quad \langle \dot{J}_y^2 \rangle = -\gamma \langle J_y^2 \rangle + \gamma \langle J_x^2 \rangle, \\ &\langle \dot{J}_z \rangle = 0; \quad \langle \dot{J}_z^2 \rangle = 0, \end{aligned} \tag{13}$$

where $J_\pm \equiv J_x + iJ_y$, so that $\langle \dot{J}_x \rangle = -(\gamma/2)\langle J_x \rangle$ and $\langle \dot{J}_y \rangle = -(\gamma/2)\langle J_y \rangle$. In the protocol for the SCAIN, we have the following values at the beginning of the squeezing process: $\langle J_x \rangle = \langle J_z \rangle = 0$, $\langle J_y \rangle = J$, $\langle J_x^2 \rangle = \langle J_z^2 \rangle = J/2$, and $\langle J_y^2 \rangle = J^2$. For $\gamma t \ll 1$, we then find that at the end of the squeezing process, we have (keeping in mind that this evolution is due to the cavity decay effect only) $\langle J_x \rangle = \langle J_z \rangle = 0$, $\langle J_y \rangle \approx J(1-\gamma t/2)$, $\langle J_z^2 \rangle = J/2$, $\langle J_x^2 \rangle = (J/2)(1+2J\gamma t)$, and $\langle J_y^2 \rangle = J^2(1-\gamma t)$, leaving the value of $\langle \mathbf{J}^2 \rangle = J(J+1)$ unchanged. Thus, we get

$$\begin{aligned} (\Delta J_x)^2 &= \langle J_x^2 \rangle - \langle J_x \rangle^2 = J/2 + J^2\gamma t, \\ (\Delta J_y)^2 &= \langle J_y^2 \rangle - \langle J_y \rangle^2 = 0, \\ (\Delta J_z)^2 &= \langle J_z^2 \rangle - \langle J_z \rangle^2 = 0. \end{aligned} \tag{14}$$

Therefore, the net effect of the cavity decay is an increase in the value of $(\Delta J_x)^2$ by an amount $J^2\gamma t$, and a decrease in the length of $\langle J_y \rangle$ by $J\gamma t/2$. We recall that in the protocol for the SCAIN, the auxiliary rotation immediately after the squeezing process maps the y component of the spins to the z component. Thus, the reduction in the length of $\langle J_y \rangle$ maps to a reduction in the length of $\langle J_z \rangle$, and therefore a reduction in the coherent signal. On the other hand, an increase in the variance of J_x does not contribute directly to an increase in the variance of the signal (which corresponds to measuring J_z). However, we allow, as an upper limit, this increase in the variance of J_x as a corresponding increase in the variance of the signal. Next, note that ideally, the initial conditions for the inverse squeezing process at $\phi = \pm\pi/(2N)$ (which is the value of the phase at which measurements are to be made, as discussed earlier) are the same as those at the beginning of the squeezing process, as can be seen in Fig. 1. Thus, we can assume that the effects of cavity decay for the inverse squeezing process are essentially the same as what we estimated above for the squeezing process. As such, for the squeezing and the inverse squeezing processes combined, we get

$$\begin{aligned} (\Delta S_{\mathrm{CAV}})^2 &= 2 * J^2\gamma t = N^2\gamma t/2, \\ \delta N_{\mathrm{CAV}} &= 2 * J\gamma t/2 = N\gamma t/2. \end{aligned} \tag{15}$$

Next, we consider the effect of spontaneous emission. As noted in the paragraph after Eq. (A5), for a large value of N, it is virtually impossible to account for the effect of spontaneous emission analytically. As such, we account for this in a heuristic manner, similar to what is done in Ref. [42]. The number of photons in the cavity is ζ^2, where ζ is given by Eq. (A8). Assuming that the atomic excited state ($|m\rangle$ in Fig. 5) decays at a rate of Γ, and that $\Delta \gg \Gamma$ as well as $\Delta \gg g$ (with g being the vacuum Rabi frequency for the cavity mode and Δ being the cavity detuning away from each atomic resonance), the number of photons scattered by each atom happens at the rate of

$$\tilde{\Gamma} = (g/\Delta)^2|\zeta|^2\Gamma = \frac{\chi}{2\mathcal{C}}\frac{(1+\tilde{\delta}^2)}{|\tilde{\delta}|}, \tag{16}$$

where $\mathcal{C}$ is the single-atom cooperativity parameter. Spontaneous emission causes the spin to flip randomly, from up to down and vice versa. Thus, the value of J_z decreases via random walk as

$$(\Delta J_z^{\mathrm{SE}})^2 \approx \mathcal{P}(1/2)N\tilde{\Gamma}t. \tag{17}$$

Here, $\mathcal{P}$ is the probability of spin flip, which is 1/2 for a symmetric system, such as the one depicted in Fig. 5, so that we get, in the limit of $|\tilde{\delta}| \ll 1$,

$$(\Delta J_z^{\mathrm{SE}})^2 \approx \frac{N\chi t}{8\mathcal{C}}|\tilde{\delta}|. \tag{18}$$

Thus, we can now write that

$$(\Delta S_{\mathrm{SE}})^2 = \frac{N\chi t}{8\mathcal{C}}|\tilde{\delta}|; \quad \delta N_{\mathrm{SE}} = \sqrt{\frac{N\chi t}{8\mathcal{C}}|\tilde{\delta}|}. \tag{19}$$

We define $\Theta \equiv \delta N/N$, where $\delta N = \delta N_{\mathrm{CAV}} + \delta N_{\mathrm{SE}}$, so that $\tilde{N} = N(1-\Theta)$. We also specify that $\chi t = \pi/2$ is the condition for creating the cat state, and assume that $\Theta \ll 1$. Inserting Eqs. (15) and (19) into Eq. (11), we then get

$$\mathcal{F} \approx \left[\frac{1}{N}(1+2\Theta) + \frac{2\pi}{N^2}(1+4\Theta)\left\{\frac{N}{|\tilde{\delta}|} + \frac{|\tilde{\delta}|}{8\mathcal{C}}\right\}\right]^{-1}. \tag{20}$$

The term inside the curly brackets in Eq. (20) is minimized for $|\tilde{\delta}| = \sqrt{8\mathcal{C}_N}$, where $\mathcal{C}_N \equiv N\mathcal{C}$ is the collective cooperativity parameter. For $\mathcal{C}_N \gg 1$ and this value of $|\tilde{\delta}|$, we get

$$\begin{aligned} &\Theta \approx [\pi^2/(32\mathcal{C}_N)]^{1/4}, \\ &\mathcal{F} \approx \left[\frac{1}{N}(1+2\Theta+8\Theta^2+32\Theta^3)\right]^{-1}. \end{aligned} \tag{21}$$

Since $\Theta \ll 1$ for $\mathcal{C}_N \gg 1$, we thus get $\mathcal{F} \approx N(1-2\Theta)$.

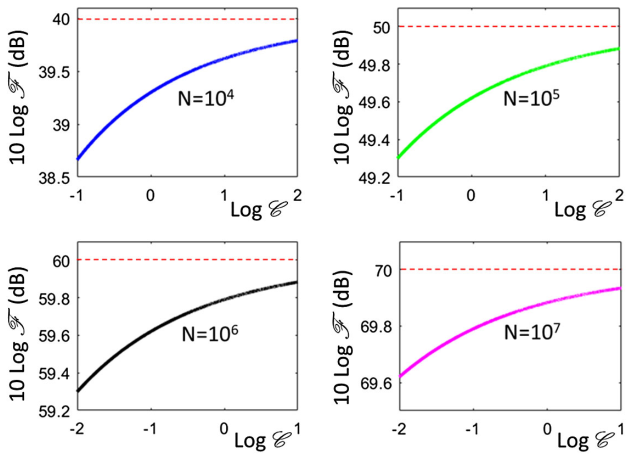

Fig. 6. Illustration of the factor of improvement $\mathcal{F}$ as a function of the cooperativity parameter $\mathcal{C}$ for four different values of N. In each case, the ideal value of $\mathcal{F}$ is indicated by the dotted red line.

In Fig. 6, we have illustrated the factor of improvement $\mathcal{F}$ as a function of the cooperativity parameter $\mathcal{C}$ for four different values of N. In each case, the ideal value of $\mathcal{F}$ is indicated by the dotted red line. As can be seen, even for $\mathcal{C} = 0.01$, which should be easily accessible, based on the analysis shown after Eq. (A12), the achievable value of $\mathcal{F}$ is within less than 1 dB of the maximum possible value of 70 dB for 10 million atoms.

In the preceding discussion, we have addressed the effect of residual spontaneous emission heuristically. This model may not account fully for the deleterious effects of spontaneous emission. Consider, for example, a situation where the centers of mass of the two components of the SC state are separated spatially by a distance $\mathcal{D}$ in the z direction. If a spontaneous emission event occurs, we will call the event "distinguishable" if, in principle, it is possible to determine which component of the SC state produced the photon; otherwise, we will call the event "indistinguishable." If the emission is distinguishable, then the SC state would collapse to a single collective state, and there would be no interference [43,44]. The distinguishability of the emission event will be determined by the size of $\mathcal{D}$. The relevant length scale here is the wavelength of the emitted photon, λ_P. For the D2 transition in Rb, $\lambda_P \approx 780$ nm. Indistinguishability would only hold for $\mathcal{D} < \lambda_P$ [14,45]. We also note here that the dephasing caused by cavity decay is also "indistinguishable," since the cavity mode is much larger than the separation between the two components of the SC state.

For the SC atomic clock mentioned earlier, as well as variations thereof for magnetometry or nuclear magnetic resonance, this condition can be easily satisfied, since the recoil corresponding to a microwave transition is very small. For example, for the hyperfine transition in the ground state of ^{87}Rb, the recoil velocity is ≈ 0.2 μm/s. As shown in Appendix A, a typical time duration for the squeezing process to produce the cat state is ≈ 0.15 μs. Thus, during the squeezing process, the value of $\mathcal{D}$ would be only ≈ 0.03 pm, far less than λ_P. Consider next the case of the SCAIN, for which the recoil velocity would be ≈ 12 mm/s. At the point of maximum separation between the two arms, the condition of $\mathcal{D} \approx \lambda_P$ would be reached for a dark zone duration of ≈ 65 μs. For a typical dark zone duration used for accelerometry or rotation sensing, which is much longer than this, the value of $\mathcal{D}$ would far exceed λ_P. However, it should be noted that the squeezing process is carried out at the onset of the splitting, and the unsqueezing happens after the two paths have come back to each other (see Fig. 2). Thus, during the squeezing/unsqueezing steps, each with a typical duration of ≈ 0.15 μs, the value of $\mathcal{D}$ would be only ≈ 1.8 nm, which is much smaller than λ_P.

One must also take into account the possibility of spontaneous emission during the pulses other than those used for squeezing and unsqueezing. For the SC atomic clock, this is not an issue, since these pulses would employ microwaves. For the SCAIN, this is important for the π pulse that reverses the direction of motion for the two arms, since the separation between the two components of the cat state would typically be much larger than λ_P at this point. However, by using strong laser fields and large detunings for each leg of the Raman transition, it should be possible to reduce the probability of a spontaneous emission during this pulse to be adequately small.

We recall that cases with only one parity (even N) contribute the signal with N-fold magnified fringes, while cases with the other parity (odd N) contribute a vanishingly small signal. While cavity decay (which is "indistinguishable," as noted above) and the "indistinguishable" spontaneous emission events would not cause a collapse of the cat state, these would change the parity of the coherent ensemble, defined as the atoms that contribute to the coherent part of the signal [as defined in Eq. (9)]. The final parity of the coherent ensemble at the end of the protocol would determine whether it would contribute to the N-fold magnified fringe signal or the vanishingly small signal.

Finally, we consider the issue of potential loss of particles due to collisions. As discussed, for example, in Refs. [43,44], this can be of potentially significant concern in creating cat states of Bose-condensed atoms. However, for the systems being considered here, the density of atoms is low enough to ignore collisions among the atoms in the cat state. Collisions with background atoms can also be made negligible by using ultrahigh vacuums produced under cryogenic conditions [46,47]. For example, in Refs. [45,48,49], which address this issue in the context of attempts to create the macroscopic superposition of nanoparticles, it has been shown that collisions with background atoms become negligible for a vacuum of $\approx 10^{-16}$ Torr. Such pressures have been previously realized in cryogenic environments [50].

6. DISCUSSION OF CLOSELY RELATED WORK

The basic concept underlying the protocol described in this paper falls within the broad category of so-called interaction-based readout (IBR) schemes [51]. A systematic discussion of the IBR schemes can be found, for example, in Ref. [19]. In this reference, many different versions of IBR schemes are discussed, including one that has similarities to the protocol described here. In another paper [21], the authors analyze an IBR scheme that also has similarities to our protocol. In Ref. [52], a systematic study is carried out to determine the maximum possible robustness against excess noise. This study concludes that our protocol, along with similar ones presented in Refs. [19,21], achieves the maximum possible sensitivity against excess noise. The optimal robustness against excess noise for a different IBR scheme employing twist-and-turn entanglement is investigated in Ref. [20]. Indeed, Refs. [20,21,52] have all cited the arXiv paper describing our protocol [35]. The authors noted in Ref. [52] that the robustness of our protocol against excess noise is ostensibly stronger than that of the corresponding protocol in Ref. [19], attributing the difference to the fact that the noise model used by us (which is akin to the one used in Ref. [11]) is different from the one used in Ref. [19]. Similarly, the robustness of our protocol is ostensibly stronger than that of the protocol in Ref. [21], for the same reason. While the maximum robustness protocols presented in Refs. [19,21] are similar to ours, we note that the details of our protocol contain significant differences and augmentations, as discussed next.

An important aspect of what we describe in this paper is the challenge in implementing this protocol for large number of cold atoms released from a magneto-optic trap. For such a scenario, the parity of the number of atoms N (i.e., whether N is even or odd) is not known. On the other hand, the protocol produces very different signals for even versus odd values of N. What we show is that one can choose to operate the protocol designed, for example, for even values of N. For instances where N is odd, this protocol will produce a vanishingly small signal so that when averaged over many instances, the net signal would correspond approximately to running the protocol for even values of N only, with the effective number of N being reduced by a factor of ~ 2. Reference [52] notes that different protocols are necessary for odd versus even values of N. However, it does not show what happens if a fixed protocol is used while the system has randomly occurring odd and even values of N. References [19,21] do not consider this issue at all.

Another important issue addressed in this paper is the application of the protocol to an atomic interferometer, where the trajectories of the two paths get physically separated spatially, thus requiring the application of an additional π pulse. We have considered the application of the protocol to this case explicitly; Refs. [19,21,52] do not consider this case. It should also be noted that in Refs. [19,52], the detection requires measurement of the population of all collective states. This is distinctly different from our protocol, where, for the case that produces the maximal robustness against excess noise, we measure the mean value of all the pseudospins in the z direction (a process referred to as conventional detection in this paper).

In Refs. [19,21,52], the robustness of the protocol against excess noise is explained by showing how the Fisher information is influenced in the presence of excess noise. While this is certainly correct, it does not seem to provide a simple and transparent reason for the robustness. In contrast, we have in this paper offered a simple explanation of the robustness, which is as follows. In this protocol, the signal fringes are amplified by a factor of N, while the quantum projection noise is magnified by a factor of $\sqrt{N}$ more than the noise under the SQL, reaching a value of N. Thus, it is clear that the classical noise would only become relevant (reducing the sensitivity by a factor of $\sqrt{2}$) when it is very large, namely, equaling N.

We also show explicitly how the measurement basis very strongly affects the robustness against excess noise. Specifically, we show that if one chooses to measure the population of one of the extremal collective states, the process is as sensitive to classical noise as conventional techniques (such a two-axis-counter-twist squeezing), so that a classical noise of unity would reduce the sensitivity by a factor of $\sqrt{2}$. In contrast, when the mean value of all the pseudospins in the z direction is measured, the excess noise has to be very large (namely, N) for the sensitivity to drop by a factor of $\sqrt{2}$.

Most important, in this paper we have addressed, in explicit and quantitative details, the critical question of the effect of dissipation during the one-axis-twist squeezing process employing an optical cavity. Specifically, we have shown, employing the cavity input–output relation and the density matrix formulation involving Langevin noise operators, how the effects of the dissipative processes are strongly suppressed due to the fact that the protocol entails phase magnification by a factor of N, and enhanced quantum noise by a factor of $\sqrt{N}$. We thus find that the maximal achievable sensitivity is very close to the ideal limit, as shown in Fig. 6. This contrasts with the findings of a similar analysis carried out in Ref. [11] for the echo squeezing protocol. In that case, the dissipation during the cavity-mediated one-axis-twist squeezing process limits the maximum achievable sensitivity to a value far below the ideal value. In Ref. [21], a brief discussion is presented regarding the effect of dissipation during the readout process only. However, this discussion is presented in the context of a generalized dissipation parameter, and does not describe the experimental conditions that would correspond to a given value of the dissipation parameter. In contrast, we have considered explicit experimental parameters, such as the cavity cooperativity parameter, the number of atoms, and the laser power in the probe, and shown that a sensitivity value very close to the ideal limit is achievable for experimentally accessible values of these parameters. References [19,52] do not address this issue of dissipation during the squeezing and unsqueezing processes.

7. CONCLUSION

Atomic precision metrology is of importance for practical applications, such as time keeping, rotation sensing, accelerometry, and magnetometry. It also plays a key role in investigations of fundamental physics, including searching for the electron's electric dipole moment, tests of general relativity, and detection of dark matter. Under ideal conditions, the sensitivity of an atomic sensor is at the SQL, dictated by the quantum projection noise. This limit can be circumvented by making use of entangled states of atoms. In particular, the use of highly entangled states can enable one to reach the HL, which represents an improvement by a factor of $\sqrt{N}$, where N is the number of atoms interrogated. However, such a process is typically more sensitive to excess noise than conventional sensors. Here we described a protocol for an atomic interferometer that can reach the HL of sensitivity while also being more insensitive to excess noise than a conventional sensor. Using spin squeezing, the sensitivity can be increased, either by lowering the quantum noise or via phase amplification, or a combination of both. In this paper, we have shown how to increase the sensitivity to the HL, while increasing the quantum noise by $\sqrt{N}$, thereby suppressing by the same factor the effect of excess noise. The protocol makes use of a SC state representing a mesoscopic superposition of two collective states of N atoms. We show that the N-fold phase magnification can be produced under two different methods of detection: one where the population of an extremal collective state is measured, and the other where the mean value of the pseudospins of all atoms is measured. However, the suppression of sensitivity to excess noise is achieved if the latter method is used, while the former method makes it extremely sensitive to excess noise. We show how the signals for a given protocol produce drastically different signals for different parities of N, for both detection methods. For a system that produces both odd and even values of N with equal probability, such as atoms released from a magneto-optic trap, we show that averaging over many instances approximately filters out the signal for one parity, thus allowing a sensitivity that is within a factor of $\sqrt{2}$ of the HL, while maintaining the robustness against excess noise. We have shown both numerical and analytical results for the ideal behavior of the SC-state-based atomic interferometer. We have also discussed potential experimental constraints for implementing this scheme, using one-axis-twist squeezing employing the cavity feedback scheme, and shown that the effects of cavity decay and spontaneous emission are highly suppressed due to the N-fold phase magnification. We have found that even for a modest value of the cavity cooperativity parameter of the order of 0.01, which should be readily accessible experimentally, the maximum improvement in sensitivity can be very close to the ideal limit for as many as 10 million atoms. We also discuss related protocols that have been proposed recently and point out the similarities and differences of these from what is proposed here. We believe that the concepts proposed here pave the way for realizing atomic interferometers—as well as other atomic sensors based on the excitation of pseudospins in an effective two-level system, such as a clock or a magnetometer—with a sensitivity very close to the HL without requiring rigorous suppression of excess noise for a range of parameters that are rather easily accessible experimentally.

APPENDIX A: EFFECTIVE EQUATIONS OF MOTION AND SCALING OF EXPERIMENTAL PARAMETERS FOR ONE-AXIS-TWIST SQUEEZING VIA CAVITY FEEDBACK

Here we derive an effective equation of motion for the one-axis-twist squeezing process employing the cavity feedback scheme, and analyze how the strength of the squeezing process scales with experimental parameters. The derivation of the effective equation of motion follows steps similar to those found in the supplement of Ref. [11]. However, we briefly repeat the essential steps here, since our notations are different, and spell out some of the steps not explicitly shown there; furthermore, there are some small, although non-critical, discrepancies between the results reported there and what we find here. For specificity, we consider ^{87}Rb as the atomic medium, with the spin-up state corresponding to the $5S_{1/2}$, $F=2$, $m_F=0$ Zeeman sublevel, and the spin-down state corresponding to the $5S_{1/2}$, $F=1$, $m_F=0$ Zeeman sublevel. The intermediate state is assumed to be the $5P_{3/2}$ manifold. We also assume the matrix element for the coupling to the intermediate state to be the same for both spin-up and spin-down states; in practice, a detailed numerical model that takes into account the choice of the polarization of the probe mode and the corresponding coupling to the relevant Zeeman sublevels for each hyperfine state within the $5P_{3/2}$ manifold has to be employed. In addition, we assume that the intermediate state decays equally, via spontaneous emission, to both ground states; again, in practice, a more detailed numerical model of spontaneous emission from all Zeeman sublevels has to be taken into account. In order to avoid the variation in the probe intensity that occurs in a standing wave cavity, it would be necessary to use a linear cavity consisting of three mirrors, as shown in Fig. 12 of Ref. [18], with one of the mirrors being a perfect reflector and each of the other two being a partial reflector. However, for simplicity of analysis, in what follows we consider a two-mirror cavity with a length of L meters, an effective mode area of A, and a reflectivity of R for each mirror. The input–output relation for such a cavity can be expressed as [53,54]

$$\dot{\hat{\tilde{a}}} = -\frac{\kappa}{2}\hat{\tilde{a}} + i\delta\hat{\tilde{a}} + \sqrt{\kappa_{\text{ex}}}\xi + \sqrt{\kappa_o}\,\hat{\tilde{f}}. \quad \textbf{(A1)}$$

Here the detuning is defined as the difference between the probe frequency (ω_p) and the cavity resonance frequency (ω_c): $\delta = \omega_p - \omega_c$. The input probe field is assumed to be classical, defined as $\alpha_{\text{in}} = \xi\exp(-i\omega_p t)$, with a mean value of $|\xi| = \sqrt{N_{\text{in}}}$, where N_{in} is the number of photons incident on the cavity in 1 s. The slowly varying amplitude of the field inside the cavity, transformed to a frame rotating at the frequency of the probe, is defined as $\hat{\tilde{a}} = \hat{a}\exp(i\omega_p t)$. The rate of decay of the intracavity intensity through the input mirror is defined as κ_{ex}, and any additional decay (including the decay through the output mirror) is defined as κ_o, so that the net rate of decay is $\kappa = \kappa_{\text{ex}} + \kappa_o$. Finally, the Langevin force operator in the last term of Eq. (A1) obeys the relations $[\hat{\tilde{f}}(t), \hat{\tilde{f}}^\dagger(t')] = \delta(t-t')$ and $\langle\hat{\tilde{f}}\rangle = 0$. Below, we assume that $\kappa_{\text{ex}} = \kappa_o = \kappa/2$, since both mirrors have the same transmissivity, and other potential losses are ignored.

The Hamiltonian for the whole system, including the atoms, the probe field inside the cavity, and the interaction among them, can be written as

$$H = H_{\text{cav}} + H_{\text{atm}} + H_{\text{int}} + H_{\text{src}}. \quad \textbf{(A2)}$$

The four components of the Hamiltonian are defined as follows [11,54] (setting $\hbar = 1$):

$$\begin{aligned} H_{\text{cav}} &= \omega_c \hat{a}^\dagger \hat{a}, \\ H_{\text{atm}} &= \sum_{j=1}^{N}[2\Delta|\uparrow\rangle\langle\uparrow|_j + (\omega_c + \Delta)|m\rangle\langle m|_j], \\ H_{\text{int}} &= \sum_{j=1}^{N}[g\hat{a}|m\rangle\langle\uparrow|_j + g\hat{a}|m\rangle\langle\downarrow|_j + \text{h.c.}], \\ H_{\text{src}} &= \sqrt{\kappa/2}[i\xi\hat{a}^\dagger e^{-i\omega_p t} - i\xi^*\hat{a}e^{i\omega_p t}], \end{aligned} \quad \textbf{(A3)}$$

where g is the vacuum Rabi frequency for the cavity mode.

The density operator ρ for the atoms and the cavity mode obeys the following equation of motion:

$$\dot{\rho} = -i[H, \rho] + D(L_{\mathrm{cd}})\rho + \sum_{j=1}^{N} D(L_{\uparrow,j})\rho + \sum_{j=1}^{N} D(L_{\downarrow,j})\rho, \tag{A4}$$

where we have defined

$$D(L)\rho = L\rho L^{\dagger} - \frac{1}{2}\{L^{\dagger}L, \rho\}. \tag{A5}$$

The Lindblad operator corresponding to cavity decay is $L_{\mathrm{cd}} = \sqrt{\kappa}\hat{a}$, and those corresponding to spontaneous emission are $L_{\uparrow} = \sqrt{\Gamma/2}|\uparrow\rangle\langle m|$ and $L_{\downarrow} = \sqrt{\Gamma/2}|\downarrow\rangle\langle m|$.

Coherent excitation of the atoms only populates the $(N+1)$ symmetric collective states [14–16]. However, the total number of collective states, including the asymmetric ones, is 2^N, the size of the Hilbert space for N two-level atoms [16]. All of these states must be taken into account when considering the effect of spontaneous emission, which can couple to both symmetric and asymmetric states. Thus, even for a modest number of N that would be relevant for a SCAIN, such an analysis is intractable. As such, we will account for the effect of spontaneous emission heuristically and exclude the Lindblad operators corresponding to spontaneous emission (this is the same approach used, for example, in Ref. [11]).

Since the probe is highly detuned with respect to the two legs of the Λ transition in Fig. 5, the intermediate state $|m\rangle$ can be eliminated adiabatically, using the approach developed in Ref. [55]. The resulting Hamiltonian then can be expressed as

$$H = (\omega_c + \epsilon\hat{J}_z)\hat{a}^{\dagger}\hat{a} + 2\Delta\hat{J}_z + \sqrt{\kappa/2}[i\xi\hat{a}^{\dagger}e^{-i\omega_p t} - i\xi^{*}\hat{a}e^{i\omega_p t}], \tag{A6}$$

where $\epsilon = 2g^2/\Delta$ is the difference between the single-photon-induced light shifts experienced by the spin-up and spin-down states, which are equal and opposite in sign. We now transform into a frame rotating at $H_A \equiv (\omega_p\hat{a}^{\dagger}\hat{a} + 2\Delta\hat{J}_z)$, which results in the following form of the Hamiltonian:

$$H = \left(-\delta + \epsilon\hat{J}_z\right)\hat{a}^{\dagger}\hat{a} + \sqrt{\kappa/2}[i\xi\hat{a}^{\dagger} - i\xi^{*}\hat{a}]. \tag{A7}$$

It is now evident from the term in the first bracket of Eq. (A7) that the detuning of the probe away from cavity resonance is modified by the light shift of the atoms. The Lindblad operator for cavity decay under this transformation picks up a time-dependent phase factor: $L_{\mathrm{cd}} = \sqrt{\kappa}\hat{a}\exp(-i\omega_p t)$. However, since the phase factor does not change $D(L_{\mathrm{cd}})\rho$ [see Eq. (A5)], we can write that effectively as $L_{\mathrm{cd}} = \sqrt{\kappa}\hat{a}$.

Next, we assume that the intracavity field can be treated as the sum of a classical field and a weak quantum field: $\hat{a} = (\alpha + \hat{q})$, where $\langle\hat{q}\rangle = 0$. We define the classical part as $\alpha = \zeta\ \exp\,(-i\omega_p t)$, so that $\langle\hat{\tilde{a}}\rangle = \zeta$. The steady-state solution of Eq. (A1) then yields (with $\kappa_{\mathrm{ex}} = \kappa/2$)

$$\zeta = \sqrt{\frac{\kappa}{2}}\frac{\xi}{(\kappa/2 - i\delta)}. \tag{A8}$$

The Hamiltonian now can be written as $H = H_a + H_b + H_c$, where

$$\begin{aligned} H_a &= -\delta\hat{q}^{\dagger}\hat{q} + \epsilon J_z[|\alpha|^2 + \hat{q}^{\dagger}\hat{q} + \alpha^{*}\hat{q} + \alpha\hat{q}^{\dagger}]\overleftrightarrow{I}, \\ H_b &= -\delta|\zeta|^2 + |\xi|^2\sqrt{\kappa/2}\left[\frac{2\delta}{\delta^2 + \kappa^2/4}\right], \\ H_c &= i(\kappa/2)\left[\alpha\hat{q}^{\dagger} - \alpha^{*}\hat{q}\right], \end{aligned} \tag{A9}$$

and the cavity-decay Lindblad operator becomes $L_{\mathrm{cd}} = \sqrt{\kappa}(\alpha + \hat{q})$. Since H_b does not involve any operators, it can be transformed out trivially, yielding $H = H_a + H_c$ and $L_{\mathrm{cd}} = \sqrt{\kappa}(\alpha + \hat{q})$. Furthermore, it can be shown easily that the equation of motion for the density matrix remains unchanged when this combination of the Hamiltonian and the cavity-decay Lindblad operator is replaced by the combination of $H = H_a$ and $L_{\mathrm{cd}} = \sqrt{\kappa}\hat{q}$.

Adiabatic elimination of the weak cavity mode $\hat{q}$, again using the approach developed in Ref. [55], yields the following expressions for the effective Hamiltonian and the Lindblad operator for the spin dynamics:

$$H = \chi J_z^2, \quad L = \sqrt{(2\chi/\tilde{\delta})}J_z, \tag{A10}$$

with the squeezing parameter χ given by

$$\chi = \tilde{\delta}(1 + \tilde{\delta}^2)^{-2}|\xi|^2\tilde{\epsilon}^2, \tag{A11}$$

where we have defined the probe detuning (away from cavity resonance) normalized to the half-width of the cavity resonance as $\tilde{\delta} \equiv \delta/(\kappa/2)$ and the single-photon-induced differential light shift for each atom normalized to the half-width of the cavity resonance as $\tilde{\epsilon} \equiv \epsilon/(\kappa/2)$. Finally, as noted earlier, the quantity $|\xi|^2$ represents the number of photons incident on the cavity per second.

An important factor that determines the degree of fidelity achievable in the squeezing process is the single-atom cooperativity, defined as $\mathcal{C} \equiv 4g^2/(\kappa\Gamma)$. In terms of this factor, the squeezing parameter can be expressed as

$$\chi = \tilde{\delta}(1 + \tilde{\delta}^2)^{-2}|\xi|^2\mathcal{C}^2(\Gamma/\Delta)^2. \tag{A12}$$

As an example, consider a linear cavity with length L, effective mode area A, and transmissivity T for each end mirror. We then find that $\mathcal{C} = \mathcal{A}/(AT)$, where $\mathcal{A} = 8\pi\hbar\omega_p\Gamma/I_{\mathrm{SAT}}$, with I_{SAT} being the saturation intensity for each leg of the Λ transition. For ^{87}Rb atoms, assuming that I_{SAT} is twice that of the cycling transition, we get $\mathcal{A} \approx 3.6 * 10^{-12}\ m^2$. For a mirror with a reflectivity of 99.999%, so that $T = T_o = 10^{-5}$, and a mode area of $(20 * 10^{-6}\ \mathrm{m})^2$, we get $\mathcal{C} \approx 900$. If we define the mode area to be D^2, and a reference value of D to be $D_o = 20 * 10^{-6}$ m, then we get $\mathcal{C} \approx 900 * (D_o/D)^2(T_o/T)$. If we denote as P the incident power, with a reference power of $P_o = 10^{-3}$ W and a reference normalized detuning of $\tilde{\delta}_o = 10^2$, we then get (in units of s^{-1})

$$\chi \approx 10^8(\tilde{\delta}_o/\tilde{\delta})^3(P/P_o)^2(D_o/D)^4(T_o/T)^2. \tag{A13}$$

Thus, for $\tilde{\delta} = \tilde{\delta}_0$, $P = P_o$, $D = D_o$ and $T = T_o$, the time needed to produce the SC state would be $t_{\mathrm{SC}} \equiv \pi/2\chi \approx 15$ ns. For a more moderate choice of parameters, e.g., $D = 10D_o$ and $T = 10T_o$, we have $\mathcal{C} \approx 0.9$ and $t_{\mathrm{SC}} \approx 15$ µs. If we increase the power to $P = 10P_o = 10^{-2}$ W, which is still very modest, we get $t_{\mathrm{SC}} \approx 0.15$ µs.

Funding. Air Force Office of Scientific Research (FA9550-09-01-0652, FA9550-18-01-0401); National Science Foundation (DGE- 0801685, DMR-1121262).

Disclosures. The authors declare no conflicts of interest.

REFERENCES

1. W. M. Itano, J. C. Bergquist, J. J. Bollinger, J. M. Gilligan, D. J. Heinzen, F. L. Moore, M. G. Raizen, and D. J. Wineland, "Quantum projection noise: Population fluctuations in two-level systems," Phys. Rev. A **47**, 3554–3570 (1993).
2. M. Kitagawa and M. Ueda, "Squeezed spin states," Phys. Rev. A **47**, 5138–5143 (1993).
3. M. H. Schleier-Smith, I. D. Leroux, and V. Vuleticć, "Squeezing the collective spin of a dilute atomic ensemble by cavity feedback," Phys. Rev. A **81**, 021804 (2010).
4. I. D. Leroux, M. H. Schleier-Smith, and V. Vuleticć, "Implementation of cavity squeezing of a collective atomic spin," Phys. Rev. Lett. **104**, 073602 (2010).
5. Y.-L. Zhang, C.-L. Zou, X.-B. Zou, L. Jiang, and G.-C. Guo, "Detuning-enhanced cavity spin squeezing," Phys. Rev. A **91**, 033625 (2015).
6. M. Foss-Feig, A. J. Daley, J. K. Thompson, and A. M. Rey, "Steady-state many-body entanglement of hot reactive fermions," Phys. Rev. Lett. **109**, 230501 (2012).
7. O. Hosten, N. J. Engelsen, R. Krishnakumar, and M. A. Kasevich, "Measurement noise 100 times lower than the quantum-projection limit using entangled atoms," Nature **529**, 505–508 (2016).
8. K. Helmerson and L. You, "Creating massive entanglement of Bose-Einstein condensed atoms," Phys. Rev. Lett. **87**, 170402 (2001).
9. I. Bouchoule and K. Mølmer, "Spin squeezing of atoms by the dipole interaction in virtually excited Rydberg states," Phys. Rev. A **65**, 041803 (2002).
10. M. Zhang, K. Helmerson, and L. You, "Entanglement and spin squeezing of Bose-Einstein-condensed atoms," Phys. Rev. A **68**, 043622 (2003).
11. E. Davis, G. Bentsen, and M. Schleier-Smith, "Approaching the Heisenberg limit without single-particle detection," Phys. Rev. Lett. **116**, 053601 (2016).
12. O. Hosten, R. Krishnakumar, N. J. Engelsen, and M. A. Kasevich, "Quantum phase magnification," Science **352**, 1552–1555 (2016).
13. R. Sarkar, R. Fang, and S. M. Shahriar, "High-Compton-frequency, parity-independent, mesoscopic Schrödinger-cat-state atom interferometer with Heisenberg-limited sensitivity," Phys. Rev. A **98**, 013636 (2018).
14. R. H. Dicke, "Coherence in spontaneous radiation processes," Phys. Rev. **93**, 99–110 (1954).
15. F. T. Arecchi, E. Courtens, R. Gilmore, and H. Thomas, "Atomic coherent states in quantum optics," Phys. Rev. A **6**, 2211–2237 (1972).
16. R. Sarkar, M. E. Kim, R. Fang, Y. Tu, and S. M. Shahriar, "Effects of non-idealities and quantization of the center of mass motion on symmetric and asymmetric collective states in a collective state atomic interferometer," J. Mod. Opt. **62**, 1253–1263 (2015).
17. M. E. Kim, R. Sarkar, R. Fang, and S. M. Shahriar, "N-atom collective-state atomic clock with $\sqrt{N}$-fold increase in effective frequency and $\sqrt{N}$-fold reduction in fringe width," Phys. Rev. A **91**, 063629 (2015).
18. R. Sarkar, M. E. Kim, R. Fang, and S. M. Shahriar, "N-atom collective-state atomic interferometer with ultrahigh Compton frequency and ultrashort de Broglie wavelength, with $\sqrt{N}$ reduction in fringe width," Phys. Rev. A **92**, 063612 (2015).
19. S. P. Nolan, S. S. Sziget, and S. A. Haine, "Optimal and robust quantum metrology using interaction-based readouts," Phys. Rev. Lett. **119**, 193601 (2017).
20. S. S. Mirkhalaf, S. P. Nolan, and S. Haine, "Robustifying twist-and-turn entanglement with interaction-based readout," Phys. Rev. A **97**, 053618 (2018).
21. J. Huang, M. Zhuang, B. Lu, Y. Ke, and C. Lee, "Achieving Heisenberg-limited metrology with spin cat states via interaction-based readout," Phys. Rev. A **98**, 012129 (2018).
22. C. J. Bordé, "Atomic interferometry with internal state labelling," Phys. Lett. A **140**, 10–12 (1989).
23. M. Kasevich and S. Chu, "Atomic interferometry using stimulated Raman transitions," Phys. Rev. Lett. **67**, 181–184 (1991).
24. F. Riehle, T. Kisters, A. Witte, J. Helmcke, and C. J. Bordé, "Optical Ramsey spectroscopy in a rotating frame: Sagnac effect in a matter-wave interferometer," Phys. Rev. Lett. **67**, 177–180 (1991).
25. M. S. Shahriar, P. Pradhan, Y. Tan, M. Jheeta, J. Morzinski, and P. R. Hemmer, "Demonstration of a continuously guided atomic interferometer using a single-zone optical excitation," J. Opt. Soc. Am. B **22**, 1566–1570 (2005).
26. M. S. Shahriar, M. Jheeta, Y. Tan, P. Pradhan, and A. Gangat, "Continuously guided atomic interferometry using a single-zone optical excitation: theoretical analysis," Opt. Commun. **243**, 183–201 (2004).
27. M. S. Shahriar, P. R. Hemmer, D. P. Katz, A. Lee, and M. G. Prentiss, "Dark-state-based three-element vector model for the stimulated Raman interaction," Phys. Rev. A **55**, 2272–2282 (1997).
28. D. B. Hume, C. W. Chou, T. Rosenband, and D. J. Wineland, "Preparation of Dicke states in an ion chain," Phys. Rev. A **80**, 052302 (2009).
29. A. Sorensen and K. Molmer, "Entanglement and quantum computation with ions in thermal motion," Phys. Rev. A **62**, 022311 (2000).
30. D. Leibfried, M. D. Barrett, T. Schaetz, J. Britton, J. Chiaverini, W. M. Itano, J. D. Jost, C. Langer, and D. J. Wineland, "Toward Heisenberg-limited spectroscopy with multiparticle entangled states," Science **304**, 1476–1478 (2004).
31. D. Leibfried and D. J. Wineland, "Efficient eigenvalue determination for arbitrary Pauli products based on generalized spin-spin interactions," J. Mod. Opt. **65**, 774–779 (2018).
32. T. Monz, P. Schindler, J. T. Barreiro, M. Chwalla, D. Nigg, W. A. Coish, M. Harlander, W. Hänsel, M. Hennrich, and R. Blatt, "14-qubit entanglement: creation and coherence," Phys. Rev. Lett. **106**, 130506 (2011).
33. D. Leibfried, E. Knill, S. Seidelin, J. Britton, R. B. Blakestad, J. Chiaverini, D. B. Hume, W. M. Itano, J. D. Jost, C. Langer, and R. Ozeri, "Creation of a six-atom 'Schrödinger cat' state," Nature **438**, 639–642 (2005).
34. E. Schrödinger, "Die gegenwärtige Situation in der Quantenmechanik," Naturwissenschaften **23**, 807–812, 823–828, 844–849 (1935). English translation by J. D. Trimmer, "The present situation in quantum mechanics: a translation of Schrödinger's 'cat paradox' paper," Proc. Am. Philos. Soc. 124, 323 (1980).
35. R. Fang, R. Sarkar, and M. S. Shahriar, "Enhancing sensitivity of an atom interferometer to the Heisenberg limit using increased quantum noise," arXiv:1707.08260 (2017).
36. M. Takeuchi, S. Ichihara, T. Takano, M. Kumakura, T. Yabuzaki, and Y. Takahashi, "Spin squeezing via one-axis twisting with coherent light," Phys. Rev. Lett. **94**, 023003 (2005).
37. I. D. Leroux, M. H. Schleier-Smith, and V. Vuletić, "Orientation-dependent entanglement lifetime in a squeezed atomic clock," Phys. Rev. Lett. **104**, 250801 (2010).
38. M. Wang, W. Qu, P. Li, H. Bao, V. Vuletić, and Y. Xiao, "Two-axis-twisting spin squeezing by multipass quantum erasure," Phys. Rev. A **96**, 013823 (2017).
39. Y. C. Liu, Z. F. Xu, G. R. Jin, and L. You, "Spin squeezing: transforming one-axis twisting into two-axis twisting," Phys. Rev. Lett. **107**, 013601 (2011).
40. L. I. R. Gil, R. Mukherjee, E. M. Bridge, M. P. A. Jones, and T. Pohl, "Spin squeezing in a Rydberg lattice clock," Phys. Rev. Lett. **112**, 103601 (2014).
41. M. S. Shahriar, Y. Wang, S. Krishnamurthy, Y. Tu, G. S. Pati, and S. Tseng, "Evolution of an N-level system via automated vectorization of the Liouville equations and application to optically controlled polarization rotation," J. Mod. Opt. **61**, 351–367 (2014).
42. M. Schleier-Smith, I. D. Leroux, and V. Vuletic, "Squeezing the collective spin of a dilute atomic ensemble by cavity feedback," Phys. Rev. A **81**, 021804 (2010).
43. Y. P. Huang and M. G. Moore, "Creation, detection, and decoherence of macroscopic quantum superposition states in double-well Bose-Einstein condensates," Phys. Rev. A **73**, 023606 (2006).

44. K. Pawłowski, M. Fadel, P. Treutlein, Y. Castin, and A. Sinatra, “Mesoscopic quantum superpositions in bimodal Bose-Einstein condensates: decoherence and strategies to counteract it,” Phys. Rev. A **95**, 063609 (2017).
45. O. Romero-Isart, “Quantum superposition of massive objects and collapse models,” Phys. Rev. A **84**, 052121 (2011).
46. P. A. Willems and K. G. Libbrecht, “Creating long-lived neutral-atom traps in a cryogenic environment,” Phys. Rev. A **51**, 1403–1406 (1995).
47. The ALPHA Collaboration, “Confinement of antihydrogen for 1,000 seconds,” Nat. Phys. **7**, 558–564 (2011).
48. O. Romero-Isart, “Coherent inflation for large quantum superpositions of levitated microspheres,” New J. Phys. **19**, 123029 (2017).
49. H. Pino, J. Prat-Camps, K. Sinha, B. P. Venkatesh, and O. Romero-Isart, “On-chip quantum interference of a superconducting microsphere,” Quantum Sci. Technol. **3**, 025001 (2018).
50. G. Gabrielse, X. Fei, L. A. Orozco, R. L. Tjoelker, J. Haas, H. Kalinowsky, T. A. Trainor, and W. Kells, “Thousandfold improvement in the measured antiproton mass,” Phys. Rev. Lett. **65**, 1317–1320 (1990).
51. L. Pezzè, A. Smerzi, M. K. Oberthaler, R. Schmied, and P. Treutlein, “Quantum metrology with nonclassical states of atomic ensembles,” Rev. Mod. Phys. **90**, 035005 (2018).
52. S. Haine, “Using interaction-based readouts to approach the ultimate limit of detection-noise robustness for quantum-enhanced metrology in collective spin systems,” Phys. Rev. A **98**, 030303 (2018).
53. C. W. Gardiner and C. M. Collett, “Input and output in damped quantum systems: quantum stochastic differential equations and the master equation,” Phys. Rev. A **31**, 3761–3774 (1985).
54. M. Aspelmeyer, T. J. Kippenberg, and F. Marquardt, “Cavity optomechanics,” Rev. Mod. Phys. **86**, 1391–1452 (2014).
55. F. Reiter and A. S. Sorensen, “Effective operator formalism for open quantum systems,” Phys. Rev. A **85**, 032111 (2012).